High-Fat Diet Induces Inflammation of Meibomian Gland

Jinghua Bu,[1–4] Minjie Zhang,[1] Yang Wu,[1,5] Nan Jiang,[1] Yuli Guo,[1] Xin He,[1] Hui He,[1] M. Vimalin Jeyalatha,[1] Peter Sol Reinach,[6] Zuguo Liu,[1,3] and Wei Li[1,3]

[1]Department of Ophthalmology, Xiang'an Hospital of Xiamen University, Xiamen, Fujian, China
[2]Fujian Provincial Key Laboratory of Ophthalmology and Visual Science, Xiamen, Fujian, China
[3]Eye Institute of Xiamen University, Xiamen, Fujian, China
[4]School of Medicine, Xiamen University, Xiamen, Fujian, China
[5]Xiamen Branch, Zhongshan Hospital, Fudan University, Xiamen, Fujian, China
[6]School of Ophthalmology and Optometry and Eye Hospital, Wenzhou Medical University, Wenzhou, Zhejiang, China

Correspondence: Wei Li, Eye Institute of Xiamen University, 4th Floor, 4221-122, Xiang'an South Road, Xiamen 361102 Fujian, China; wei1018@xmu.edu.cn.

JB, MZ, and YW contributed equally to this work and should therefore be regarded as co-first authors.

Received: January 21, 2021
Accepted: July 20, 2021
Published: August 16, 2021

Citation: Bu J, Zhang M, Wu Y, et al. High-fat diet induces inflammation of meibomian gland. *Invest Ophthalmol Vis Sci.* 2021;62(10):13. https://doi.org/10.1167/iovs.62.10.13

Purpose. To determine if a high-fat diet (HFD) induces meibomian gland (MG) inflammation in mice.

Methods. Male C57BL/6J mice were fed a standard diet (SD), HFD, or HFD supplemented with the peroxisome proliferator-activated receptor gamma (PPAR-γ) agonist rosiglitazone for various durations. Body weight, blood lipid levels, and eyelid changes were monitored at regular intervals. MG sections were subjected to hematoxylin and eosin staining, LipidTox staining, TUNEL assay, and immunostaining. Quantitative RT-PCR and western blot analyses were performed to detect relative gene expression and signaling pathway activation in MGs.

Results. MG acinus accumulated more lipids in the mice fed the HFD. Periglandular CD45-positive and F4/80-positive cell infiltration were more evident in the HFD mice, and they were accompanied by upregulation of inflammation-related cytokines. PPAR-γ downregulation accompanied activation of the mitogen-activated protein kinase (MAPK) and nuclear factor kappa B (NF-κB) signaling pathways in the HFD mice. There was increased acini cell apoptosis and mitochondria damage in mice fed the HFD. MG inflammation was ameliorated following a shift to the standard diet and rosiglitazone treatment in the mice fed the HFD.

Conclusions. HFD-induced declines in PPAR-γ expression and MAPK and NF-κB signaling pathway activation resulted in MG inflammation and dysfunction in mice.

Keywords: high-fat diet, hyperlipidemia, meibomian gland, inflammation, PPAR-γ

Hyperlipidemia refers to an abnormality in lipid metabolism, which is characterized by an increase in total cholesterol, triglycerides, and low-density lipoprotein cholesterol and/or a decrease in circulating high-density lipoprotein cholesterol.[1] In the United States, more than 100 million (about 53% of adults) have elevated low-density lipoprotein cholesterol levels,[2] and approximately 31 million American adults have total cholesterol levels that exceed 240 mg/dL.[3] Globally, hyperlipidemia is associated with more than half of ischemic heart disease,[4] and it has been considered to be a major risk factor contributing to the prevalence and severity of coronary heart diseases.[5] Hyperlipidemia is also involved in augmenting comorbidities such as type 2 diabetes mellitus, hypertension, nonalcoholic fatty liver disease, and atherosclerosis.[6] It has become a major global health challenge leading to high overall medical and nonmedical expenditures.[7]

Our recent study has shown that hyperlipidemic mice fed a high-fat diet (HFD) showed dry eye–like ocular surface damage.[8] Another study from our group found that apolipoprotein E knockout (*ApoE*$^{-/-}$) mice, which were characterized by severe hyperlipidemia, demonstrated a pathological change in meibomian gland dysfunction (MGD).[9] *ApoE*$^{-/-}$ mice showed extreme hyperlipidemia of greater than 700 mg/dL of cholesterol in serum,[9] which is not common in patients with hyperlipidemia (generally over 200 mg/dL in serum).[10] In the current study, we induced a hyperlipidemia model by feeding C57BL/6J mice a HFD, which resulted in cholesterol levels similar to those of moderate hyperlipidemia in humans, to investigate MG changes under hyperlipidemia conditions. We found that hyperlipidemia induced inflammation of the MG and surrounding microenvironment. Furthermore, this condition is mediated through activation of the mitogen-activated protein kinase (MAPK) and nuclear factor kappa B (NF-κB) signaling pathways, as well as downregulation of peroxisome proliferator-activated receptor gamma (PPAR-γ) expression. Our study may reveal therapeutic targets for hyperlipidemia-induced MGD.

Materials and Methods

Materials

PPAR-γ (ab45036), interleukin (IL)-1β (ab9722), tumor necrosis factor-alpha (TNF-α; ab66579), and F4/80 (ab6640)

antibodies were obtained from Abcam (Cambridge, UK). CD45 antibody (sc-52491) and rosiglitazone (sc-202795) were obtained from Santa Cruz Biotechnology (Dallas, TX, USA). IL-6 (12912S), NF-κB p65 (8242), phospho-NF-κB p65 (3033), stress-activated protein kinase (SAPK)/Jun-amino-terminal kinase (JNK; 9258), phospho-SAPK/JNK (9255S), p38 MAPK (9212L), phospho-p38 MAPK (4631L), p44/42 MAPK (Erk1/2) (4695S), and phospho-p44/42 MAPK (Erk1/2) (9101S) antibodies were obtained from Cell Signaling Technology (Danvers, MA, USA). Invitrogen Donkey anti-Goat IgG (H+L) Cross-Adsorbed Secondary Antibody, Alexa Fluor 594 (A-11058); Invitrogen Donkey anti-Goat IgG (H+L) Cross-Adsorbed Secondary Antibody, Alexa Fluor 488 (A-11055); and Donkey anti-Rabbit IgG (H+L) Highly Cross-Adsorbed Secondary Antibody (A-21206) were obtained from Thermo Fisher Scientific (Waltham, MA, USA). Horseradish peroxidase (HRP)-conjugated anti-β-actin antibody (a5316) was obtained from Sigma-Aldrich (St. Louis, MO, USA), and 4′,6-diamidino-2-phenylindole (DAPI; H-1200) and mounting medium (H-5000) were obtained from Vector Laboratories (Burlingame, CA, USA).

Animals

Male C57BL/6J mice (4 weeks old) were purchased from Shanghai SLAC Laboratory Animal Center (Shanghai, China). All studies were performed in accordance with the ARVO Statement for the Use of Animals in Ophthalmic and Vision Research. The experimental protocol was approved by the animal ethics committee of Xiamen University. Mice were housed in a standard pathogen-free environment at 25°C ± 1°C and 60% ± 10% relative humidity on an alternating 12-hour light/dark cycles from 8:00 AM to 8:00 PM. Two groups of 4-week-old mice were fed with a standard diet (SD, 10 kcal% fat, 1022; Beijing HFK Bioscience, Beijing, China) or a HFD (60 kcal% fat, D12492; Research Diets, New Brunswick, NJ, USA). They were sacrificed at various times ranging from 4 weeks to 16 weeks. Another group of mice (HFD-rosi) was intraperitoneally injected with rosiglitazone (10 mg/kg/d, one time daily) over the course of 4 weeks and were fed a HFD. The HFD-rev group were first fed a HFD for 4 weeks, followed by a SD for another 4 weeks. Each group at each time point included 20 mice.

Plasma Cholesterol Measurements

Blood was collected from mice on the HFD at various time points after 8 hours of fasting ($n = 5$ for each group). Plasma total cholesterol was then measured enzymatically using a commercially available kit (ab65390; Abcam).

Slit-Lamp Examination

The animals were weighed and photographed; the eyelid margins and corneas were then imaged under a slit-lamp microscope (Takagi Seiko Co., Ltd., Nagano, Japan) by a single masked ophthalmologist.

Histological Analysis

Eyelid tissues ($n = 5$ for each group) were embedded in optimal cutting temperature (OCT) compound or paraffin according to the standard protocol. OCT-embedded samples were cut into 5-µm-thick sections, mounted on glass slides, and stored at –80°C. Hematoxylin and eosin (H&E) staining (three sections per animal, five animals per group) was performed on the paraffin sections. For the transmission electron microscopy analysis, MG tissues (three sections per animal, five animals per group) were fixed in a mixture of 2.5% glutaraldehyde and 4% paraformaldehyde in PBS (pH 7.4) at 4°C for 2 hours, and they were then cut into pieces 4 mm long by 2 mm wide. After that, they were dehydrated, embedded, sliced, and stained using a standard protocol as we have previously reported.[11] The MG ultrastructure was observed under a transmission electron microscope (JEM2100HC; JEOL, Tokyo, Japan).

LipidTox Staining

Eyelid frozen sections ($n = 5$ for each group) were fixed in 4% paraformaldehyde for 30 minutes and washed in PBS for 5 minutes. Sections were then stained with Invitrogen HCS LipidTOX (1:250, H34475; Thermo Fisher Scientific) for 1 hour at room temperature. After rinsing with PBS for 10 minutes, the sections were counterstained with DAPI. Digital images of representative areas of the MG were captured with a Leica upright microscope (DM2500; Leica Microsystems, Wetzlar, Germany). The mean intensity of staining in sections was measured by image analysis software (NIS Elements 4.1; Nikon, Melville, NY, USA).

Immunofluorescent Staining

Frozen sections ($n = 5$ for each group) were fixed in 4% paraformaldehyde for 10 minutes and then incubated at 4°C overnight with primary antibodies for IL-1β (1:150), TNF-α (1:200), F4/80 (1:200), CD45 (1:150), and IL-6 (1:200). Negative controls were generated simultaneously by incubating sections with PBS without a primary antibody. On the next day, samples were incubated with Alexa Fluor 594-conjugated IgG (1:300) or Alexa Fluor 488-conjugated IgG (1:300) for 1 hour in the dark at room temperature followed by three PBS washes and counterstaining with DAPI. Digital images of representative areas of the MG were captured with a Leica upright microscope (DM2500; Leica Microsystems, Wetzlar, Germany).

TUNEL Assay

Cell apoptosis detection was performed using the DeadEnd Fluorometric TUNEL System (G3250; Promega, Fitchburg, WI, USA). The MG frozen sections ($n = 5$ for each group) were incubated with proteinase-K Tris/HCL, pH = 7.4 (10 mM), for 30 minutes at 37°C, followed by three washes with PBS for 5 minutes each. Then, 50 µL of a TUNEL reaction mixture was added, and the sections were placed in the dark for 1 hour at 37°C. The specimens were rinsed three times with PBS for 5 minutes each, counterstained with DAPI, and photographed with a Leica upright microscope (DM2500; Leica Microsystems, Wetzlar, Germany).

RNA Extraction and Quantitative RT-PCR

MGs were isolated by removing skin, subcutaneous tissue, muscle, and palpebral conjunctiva under a dissecting microscope. Total RNA was extracted from the samples using Invitrogen TRIzol reagent (15596-018; Thermo Fisher Scientific). Every group had five samples, and each sample consisted

Investigative Ophthalmology & Visual Science

Table. Mouse Primer Sequences Used for Quantitative RT-PCR

Gene	Sense Primer	Anti-Sense Primer
IL-1β	5′-GGCAACTGTTCCTGAACTCAACTG-3′	5′-CCATTGAGGTGGAGAGCTTTCAGC-3′
IL-6	5′-GAGGATACCACTCCCAACAGACC-3′	5′-AAGTGCATCATCGTTGTTCATACA-3′
IL-10	5′-GCCAGTACAGCCGGGAAGACAATA-3′	5′-GCCTTGTAGACACCTTGGTCTT-3′
TNF-α	5′-AGCCCACGTAGCAAACCACCAA-3′	5′-ACACCCATTCCCTTCACAGAGCAAT-3′
MMP-3	5′-CCTTTTGATGGGCCTGGAAC-3′	5′-GAGTGGCCAAGTTCATGAGC-3′
MMP-9	5′-CAATCCTTGCAATGTGGATG-3′	5′-AGTAAGGAAGGGGCCCTGTA-3′
PPAR-γ	5′-CCGAAGAACCATCCGATT-3′	5′-CGGGAAGGACTTTATGTA-3′
β-actin	5′-CCTAAGGCCAACCGTGAAAAG-3′	5′-AGGCATACAGGGACAGCACAG-3′

of pooled MG tissues from both eyes of the same mouse. An equal amount of RNA was reverse transcribed to cDNA using a reverse-transcription kit (RR047A; TaKaRa, Shiga, Japan) following the manufacturer's protocol. Real-time PCR was performed with a StepOne Real-Time PCR detection system (Applied Biosystems, Alameda, CA, USA) and with a SYBR Premix Ex Taq Kit (RR420A; TaKaRa) according to the manufacturer's instructions. The Table provides the primer sequences used to amplify specific gene products. The amplification program included an initial denaturation step at 95°C for 10 minutes, followed by denaturation at 95°C for 10 seconds and annealing and extension at 60°C for 30 seconds for 40 cycles, after which a melt curve analysis was conducted to confirm amplification specificity. Differential gene expression was calculated according to the comparative threshold cycle method and normalized to β-actin expression as the reference gene.

Western Blot Analysis

Isolated MGs were extracted in a cold lysis buffer composed of protease and phosphatase inhibitors (78440; Thermo Fisher Scientific). Protein concentration was quantified using a BCA Protein Assay Kit (23225; Thermo Fisher Scientific). Each group contained five samples, and each sample consisted of pooled MGs from both eyes of the same mouse. Equal amounts of protein extracts (20 µg) were subjected to electrophoresis on 10% tricine gels and then electrophoretically transferred to a polyvinylidene fluoride membrane. After blocking in 5% BSA for 1 hour, the membranes were incubated overnight at 4°C with one of the following primary antibodies: PPAR-γ (1:1000), NF-κB p65 (1:1000), phospho-NF-κB p65 (1:1000), SAPK/JNK (1:2000), phospho-SAPK/JNK (1:2000), p38 MAPK (1:2000), phospho-p38 MAPK (1:2000), p44/42 MAPK (Erk1/2; 1:1000), phospho-p44/42 MAPK (Erk1/2; 1:1000), or β-actin (1:8000). After three washes with Tris-buffered saline containing 0.05% Tween 20 for 10 minutes, the membranes were incubated with HRP-conjugated goat anti-mouse or anti-rabbit IgG secondary antibodies. HRP-conjugated mouse anti–β-actin was used for protein quantification. An enhanced chemiluminescence reagent (ECL-500; Lulong, Inc., Xiamen, China) and a transilluminator (ChemiDoc XRS System; Bio-Rad, Philadelphia, PA, USA) were used to determine the protein expression levels.

Statistical Analysis

Statistical analysis was performed with SPSS Statistics 16.0 (IBM, Armonk, NY, USA). Summary data are reported as means ± SD. The Mann–Whitney test was conducted for statistical comparisons among groups using Prism 6.0 software (GraphPad Software, San Diego, CA, USA). $P < 0.05$ was considered statistically significant.

Results

HFD Induces Abnormalities in MG Secretion

Mice on the 16-week HFD showed significant increases in their body size (Fig. 1A), body mass (Fig. 1B), and blood total cholesterol levels (Fig. 1C), which were higher than for their counterparts on a SD. Slit-lamp microscope imaging showed milky secretions on the eyelid margins of mice after 4 weeks of the HFD, as well as in the conjunctival sac after 8 weeks of the HFD. The secretions became more prominent after 12 and 16 weeks (Fig. 1D).

HFD Induces Histological and Functional MG Changes

In the HFD group, obvious periglandular neutrophils and monocytes/macrophages appeared beginning at 8 weeks (Fig. 2A). LipidTox staining demonstrated increased condensed fluorescence in the acinar units of the HFD group between 4 weeks and 16 weeks, whereas diffuse and less pronounced staining patterns were observed in mice in the SD group (Fig. 2B), suggesting that the HFD induced lipid distribution changes in the MG.

HFD Induces Proinflammatory Cytokines Expression and Inflammatory Cell Infiltration in the MG Surrounding Microenvironment

To further determine the inflammatory condition of the MG after a HFD, we performed immunofluorescent staining of several proinflammatory cytokines. The results showed that IL-1β (Fig. 3A), TNF-α (Fig. 3B), and IL-6 (Fig. 3C) expression was obviously higher in the HFD group than in the SD group from 4 weeks to 16 weeks. Furthermore, CD45 (Fig. 3A) and F4/80 (Fig. 3B) immunofluorescent staining was more intense in the MGs of mice fed the HFD than those of the SD mice, indicating more pan-leukocyte and macrophage infiltration in the HFD group. In addition, IL-1β, TNF-α, matrix metalloproteinase-3 (MMP-3), and IL-10 mRNA levels were also generally higher in the HFD group compared with their corresponding levels in the SD group at different stages between 4 weeks and 16 weeks (Fig. 3D). IL-6 mRNA was only increased after 4 weeks of the HFD. MMP-9 was lower for the HFD at 4 weeks but increased from 8 weeks to 12 weeks, and there was no increase at 16 weeks compared with the SD group (Fig. 3D). These results confirmed that the HFD induced chronic inflammation of the MG microenvironment.

Investigative Ophthalmology & Visual Science

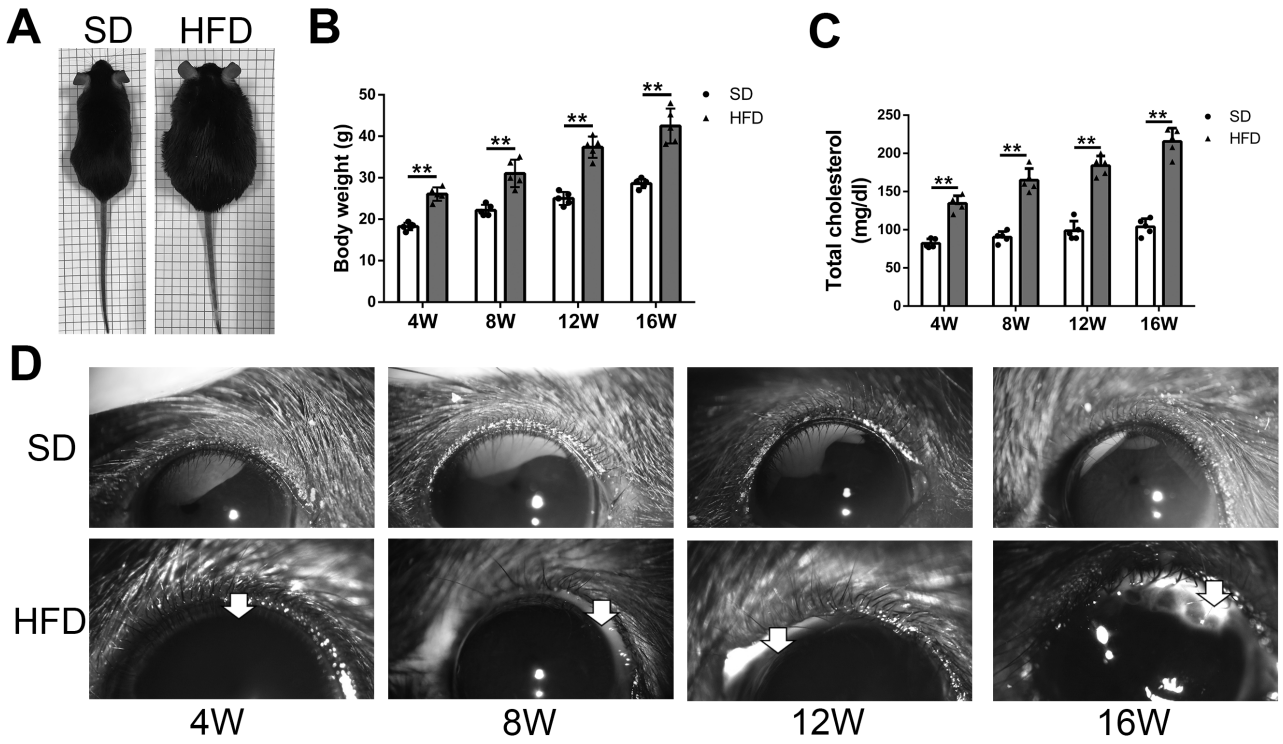

Figure 1. HFD-induced hyperlipidemia accompanied eyelid margin secretion abnormalities. The body size of mice fed a HFD for 16 weeks was significant larger compared with mice fed the SD for the same feeding time (**A**). Body mass (**B**) and total cholesterol concentrations (**C**) significantly increased in mice placed on the HFD compared with SD mice. Representative slit-lamp images show a milky secretions (*white arrows*) in the eyelid margins of mice placed on the HFD, especially after 16 weeks of being on this regimen (**D**). Data are shown as mean ± SD; $n = 5$; $^{**}P < 0.01$.

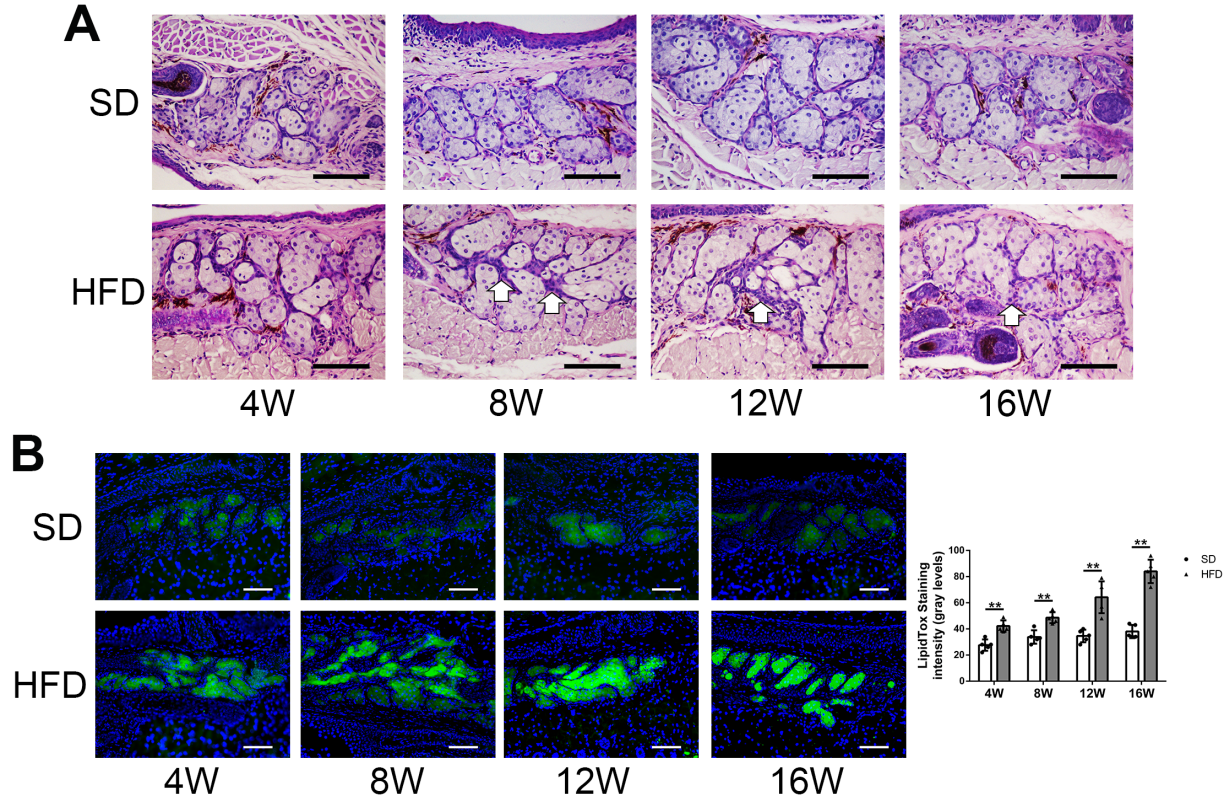

Figure 2. The HFD induced MG histological changes. Representative H&E staining of eyelids shows obvious neutrophils and monocytes/macrophages around the MG acini in mice on the HFD from 8 weeks (**A**, *white arrows*). LipidTox staining shows condensed lipid accumulation in the MG of mice fed the HFD (**B**, **C**). *Scale bars*: 50 µm (**A**), 100 µm (**B**); $n = 5$; $^{**}P < 0.01$.

Investigative Ophthalmology & Visual Science

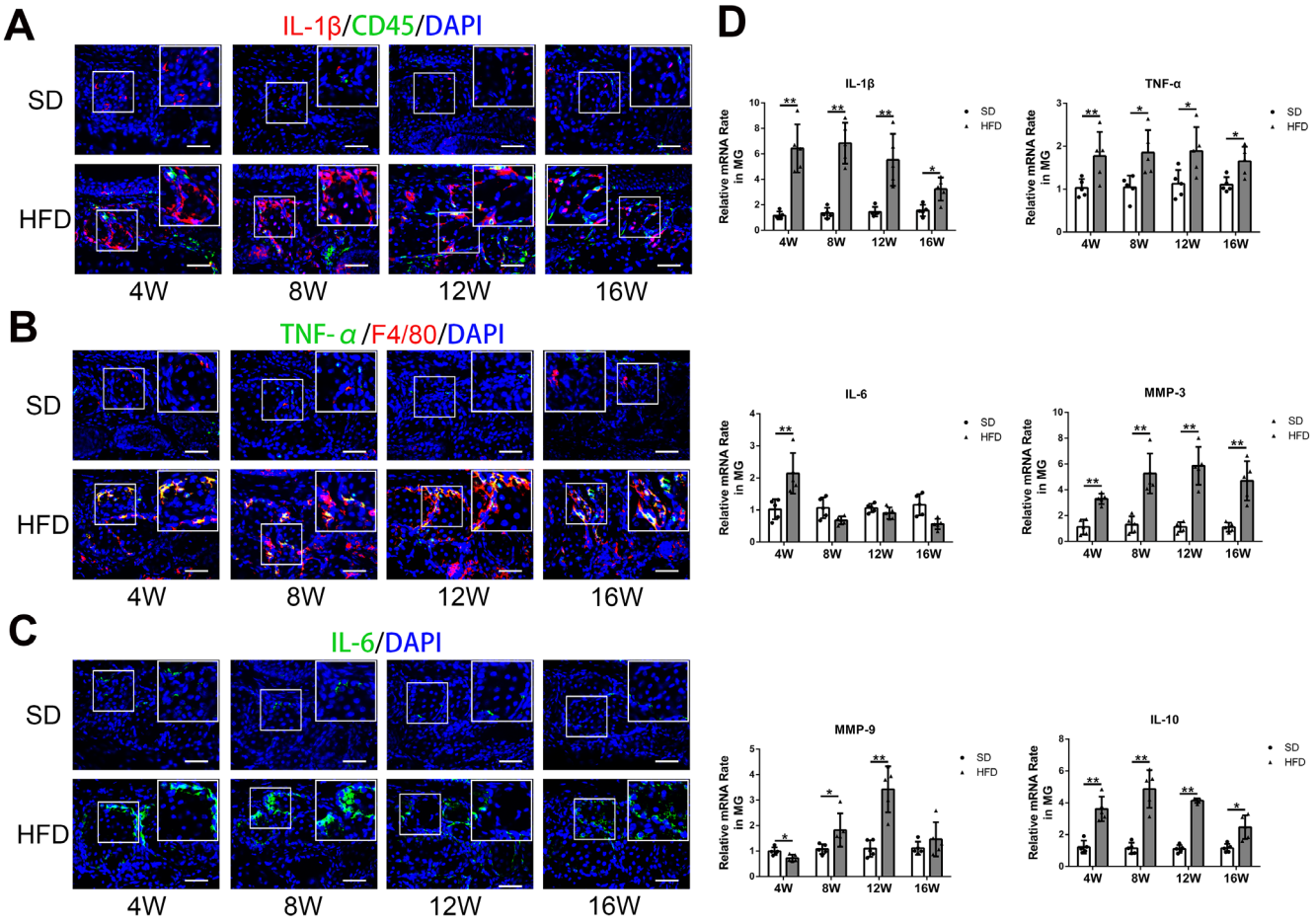

Figure 3. The HFD induced inflammatory cell infiltration and increases in proinflammatory cytokine levels. (**A–C**) Immunofluorescent staining shows increased IL-1β, CD45, TNF-α, F4/80, and IL-6 expression levels in the MG of mice fed the HFD. (**D**) Gene expression levels of IL-1β, IL-6, TNF-α, MMP-3, MMP-9, and IL-10 were upregulated in the MG of mice placed on the HFD (D). *Scale bars*: 50 µm. Data are shown as mean ± SD; $n = 5$; $^{*}P < 0.05$, $^{**}P < 0.01$.

PPAR-γ Expression Was Downregulated in HFD Mice

PPAR-γ plays an important role in mediating MG morphogenesis and meibocyte differentiation and is also a major regulator of lipid synthesis.[12] PPAR-γ agonists inhibit proinflammatory cytokine production in monocytes and macrophages.[13] These effects include declines in TNF-α, IL-1β, IL-6, and IL-12 expression levels, as well as inhibition of inducible nitric oxide synthase and MMP-9 in monocytes and macrophages.[14] PPAR-γ upregulation is associated with declines in both the NF-κB signaling pathway and stress-induced inflammatory response.[15] Such effects of a HFD can also be found in the microbial and physiological ecosystems of the murine small intestine.[16] Consistent with this association, we found dramatic decreases of PPAR-γ gene and protein expression levels in the mouse MGs after being on the HFD for 4 to 16 weeks (Figs. 4A–4C).

HFD Upregulates Both MAPK and NF-κB Signaling Pathways

Proinflammatory cytokine responses to a variety of environmental stresses including dietary changes are induced through a host of different cell signaling pathways that mediate NF-κB activation.[17] To clarify which mediators were activated by the HFD in the MG, the phospho-NF-κB p65, phospho-JNK, phospho-extracellular signal-regulated kinase (ERK), and phospho-p38 MAPK protein expression levels were measured. The western blotting results showed that all of these pathway constituents were upregulated (Fig. 4D), based on increases in the ratios of phosphorylated protein divided by total protein for p38, ERK, JNK, and NF-κB p65 at different time points (Fig. 4E). These rises collectively indicated that p38, JNK, and ERK/MAPK cascades and their downstream NF-κB signaling pathways are involved in mediating HFD-induced inflammation of the MG.

HFD Promotes MG Apoptosis and Induces Ultrastructural Changes in MG Acinar Cells

We performed TUNEL assays on the MG tissues to identify apoptotic cells. TUNEL-positive cells were scarce in the SD group but were obvious in the HFD group (Fig. 5A). Cell counting results confirmed more apoptotic cells in the MG of mice fed the HFD from 4 to 16 weeks (Fig. 5B). After 16 weeks, MG acinar cell nuclear condensation and

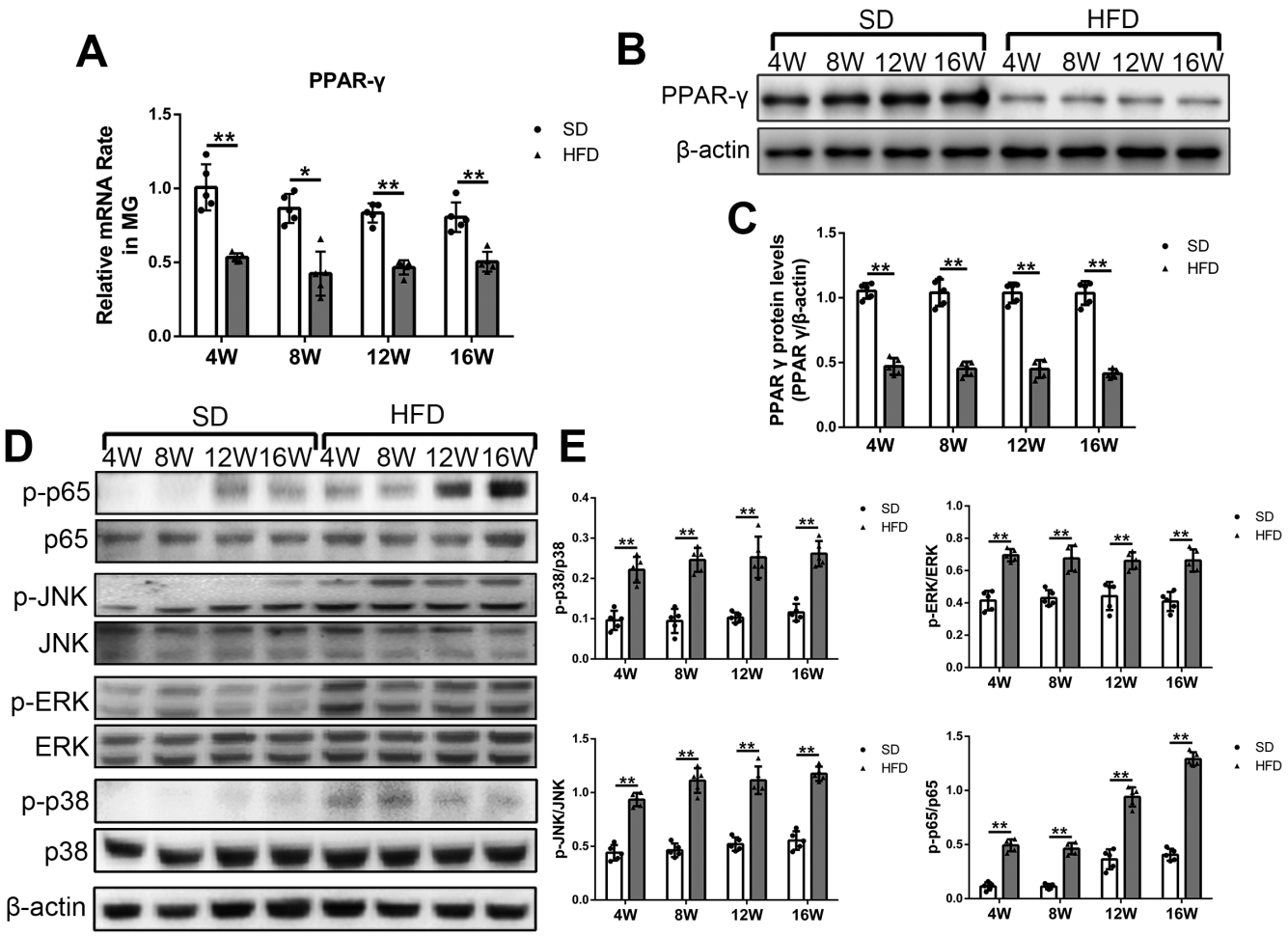

Figure 4. The HFD downregulated PPAR-γ expression and upregulated both MAPK and NF-κB signaling pathways. (**A**–**C**) Quantitative RT-PCR and western blot analysis documented declines in the PPAR-γ gene and protein expression in the MGs of mice fed the HFD. (**D**) Western blot analysis documented increases in MG MAPK and NF-κB signaling pathway phosphorylation in mice placed on the HFD. (**E**) The levels of the phosphorylated forms of MAPKs or NF-κB p65 were individually normalized to the expression levels of their total form. Data are shown as mean ± SD; $n = 5$; $^{*}P < 0.05$, $^{**}P < 0.01$.

fragmentation developed only in the HFD group (Fig. 5C-c, arrow head). Furthermore, the HFD disrupted mitochondrial structural integrity. The mitochondria were swollen with disorganized cristae (Fig. 5C-d, arrow head), in contrast to the dense and organized mitochondrial cristae in the SD group (Fig. 5C-b).

Diet Shift Alleviates MG Inflammation Induced by the HFD

To further evaluate the reversibility of HFD-induced inflammation of the MG, mice after 4 weeks of the HFD were fed with the SD for another 4 weeks while their littermates remained on the HFD. After the 4-week diet shift, IL-1β, IL-6, TNF-α, CD45, and F4/80 immunofluorescent staining, along with inflammatory cell infiltration, fell significantly below those in the HFD group (Fig. 6A). The IL-1β, TNF-α, IL-6, MMP-3, MMP-9, and IL-10 gene expression levels reverted back to those in mice fed the SD (Fig. 6B). Furthermore, the PPAR-γ gene and protein expression levels significantly increased to almost reach those of mice on the SD (Fig. 6C). Moreover, western blotting analysis showed that NF-κB p65, JNK, ERK, and p38 MAPK phosphorylation declined to levels similar to those in the SD group (Fig. 6D).

Rosiglitazone Suppresses HFD-Induced MG Inflammation

The declines in PPAR-γ gene and protein expression levels and MG phenotypic changes in the HFD group prompted us to determine if stimulating PPAR-γ with rosiglitazone, a specific PPAR-γ agonist, could reverse any of these phenotypic changes. Indeed, rosiglitazone treatment for 4 weeks upregulated PPAR-γ gene and protein expression in the MG of the HFD group (Fig. 7A). There was scant IL-1β, TNF-α, IL-6, CD45, and F4/80 immunofluorescent staining compared with that in the HFD group (Fig. 7B). Furthermore, proinflammatory IL-1β, TNF-α, and IL-6 gene expression levels were downregulated, whereas anti-inflammatory IL-10 expression was upregulated in mice after rosiglitazone treatment (Fig. 7C). Phosphorylated NF-κB p65, JNK, ERK, and p38 MAPK expression levels in the MG also decreased after rosiglitazone treatment (Fig. 7D). Therefore, PPAR-γ modulation may promote MG inflammation induced by a HFD.

Discussion

MGs are large sebaceous glands within the eyelids that can secrete lipids to stabilize tear film and reduce aqueous tear

Investigative Ophthalmology & Visual Science

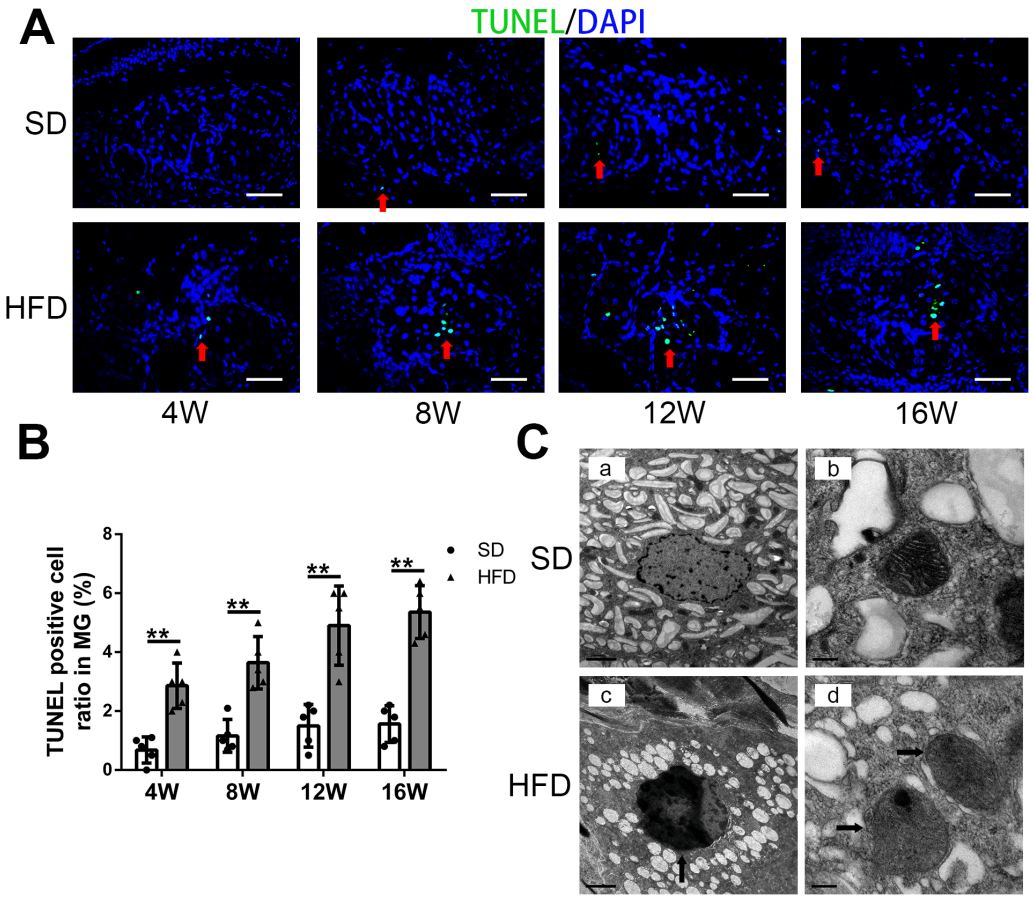

Figure 5. The HFD promoted MG apoptosis and induced ultrastructural mitochondrial alterations. (**A**) Representative images show the marked increase in apoptotic TUNEL-stained cells in mice placed on the HFD in comparison with those fed the SD. *Red arrows* indicate TUNEL-positive cells. (**B**) The TUNEL-positive cell ratios of mice fed the HFD were significantly higher than for the mice fed the SD. (**C**) Representative transmission electron microscopy images of the MG showing nuclear fragmentation and karyopyknosis in mice placed on the HFD (**C-c**, *arrowhead*) and the absence of any abnormalities in mice placed on the SD (**C-a**). Cristae in mitochondria from mice placed on the HFD are disorganized (**C-d**, *arrowhead*), whereas they appear organized in mice placed on the SD (**C-b**). *Scale bars*: 50 µm (**A**), 0.2 µm (**C**). Data are shown as mean ± SD; $n = 5$; $^{**}P < 0.01$.

evaporation.[18] MGD is a chronic and diffuse abnormality that is commonly characterized by terminal duct obstruction and/or qualitative/quantitative changes in the glandular secretory content.[19] MGD is currently considered to be a major causative factor of dry eye disease.[20]

We have shown here that a HFD induced chronic inflammatory of MG in a mouse model. This condition is mediated through activation of the MAPK and NF-κB signaling pathways and downregulation of PPAR-γ expression. The MG secretion and lipid accumulation in acini were abnormal in the mice fed the HFD, changes similar to those in other MGD animal models and patients.[21,22]

It was reported that TNF-α levels were upregulated in the adipose tissue of obese murine models,[23] and there was an association between metabolic disorders and chronic inflammation.[24] Extensive studies have demonstrated that HFD-related inflammation is characterized by the accumulation of macrophages in adipose, liver, muscle, or other tissues, resulting in elevated levels of proinflammatory IL-1, IL-6, IL-8, and TNF-α cytokines.[25–29] It is well established that adipose tissue and liver are chronically inflamed during a prolonged HFD.[30,31] Hyperlipidemia accompanying the metabolic syndrome predisposes development of a chronic inflammatory environment, possibly contributing to diabetes, cardiovascular disease, neurodegenerative disorders, and musculoskeletal system diseases.[6,32–34] With regard to ocular disorders, hyperlipidemia can disrupt ocular health by promoting cataract, maculopathy, glaucoma, and diabetic retinopathy.[35–38] Such an association was demonstrated when chronic increases in proinflammatory mediators in HFD murine models disrupted vitreous and retinal homeostasis.[39,40] Because MG is essential for maintaining ocular surface homeostasis,[15] we determined whether or not the chronic inflammatory condition induced by a HFD in mice compromises ocular surface health through pathophysiological changes in the MG. The development of HFD-related hyperlipidemia was associated with upregulation of both the MAPK-linked NF-κB signaling cassette and persistent rises in proinflammatory cytokine genes and protein expression. These rises were accompanied instead by PPAR-γ downregulation.

As previously reported, macrophages mainly produce proinflammatory cytokines, but they can also produce anti-inflammatory cytokines such as IL-10.[41,42] We found prominent macrophage infiltration in the MGs of the HFD group. Therefore, it is conceivable that IL-10 expression increases in the MG due to a HFD. Consistent with this finding, Stienstra et al.[43] demonstrated that HFD feeding could increase the

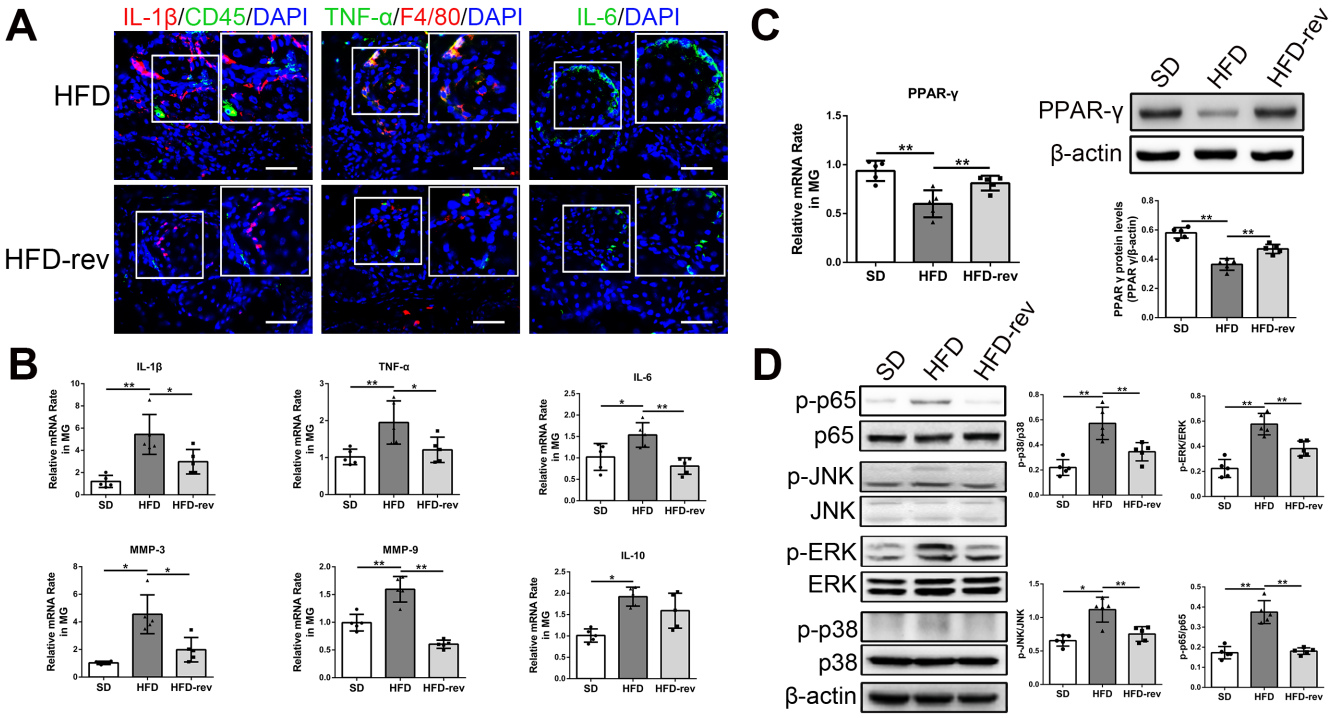

Figure 6. Diet shift alleviated MG inflammation induced by the HFD. Immunofluorescent staining of IL-1β, CD45, TNF-α, F4/80, and IL-6 shows significantly less staining following replacement of the HFD with the SD. (**A**) The levels in these HFD-rev group are compared with levels in mice placed on the SD. (**B**) This substitution of the HFD with the SD caused declines in MG IL-1β, IL-6, TNF-α, MMP-3, and MMP-9 gene expression levels, which became more similar to those in mice kept throughout the entire period on the SD. (**C**) Quantitative RT-PCR and western blot analysis documented the reversal of declines in MG PPAR-γ gene and protein expression levels subsequent to replacement of the HFD with the SD in mice. (**D**) Western blot analysis shows the declines in MAPK and p65 NF-κB phosphorylation subsequent to replacing the HFD with the SD. *Scale bars*: 50 µm. Data are shown as mean ± SD; $n = 5$; $^{*}P < 0.05$, $^{**}P < 0.01$.

expression of IL-10 in adipose tissue. Our previous study also showed that a HFD could induce IL-10 expression in lacrimal gland.[44] In the current study, IL-10 was significantly increased from 4 weeks to 8 weeks; it was attenuated from 8 weeks to 16 weeks after the HFD but was still higher than that of the SD group. We hypothesized that IL-10 may have a compensatory function in suppressing the inflammation caused by a HFD in the early stages. We noticed that IL-10 expression was upregulated in MG after rosiglitazone treatment. A previous study reported that rosiglitazone markedly increased the number of macrophages in adipose tissue and then upregulated the IL-10.[43] Rosiglitazone could also induce IL-10 expression in colitis and Parkinson's disease models.[45,46] Based on our current study, PPAR-γ is likely to continue to upregulate the expression of anti-inflammatory cytokines (such as IL-10) and decelerate the process of MGD.

MMP-9 is an inflammatory mediator of the ocular surface disease such as dry eye and conjunctivochalasis.[47] MMP-9 is also involved in the regulation of cell death. MMP-9 deficiency protects against retinal ganglion cell death.[48] Ding et al.[49] reported that 13-*cis*-retinoic acid may promote MG epithelial inflammation and cell death, in part via MMP-9. MMP-3 is a physiological activator of MMP-9.[50] In our current study, the HFD elevated the expression of MMP-3 and MMP-9 in the MG. The increase of MMP-3 and MMP-9 may be responsible, at least in part, for the HFD-induced MG inflammation and cell apoptosis.

Lipid accumulation induced by a HFD is known to induce inflammation through activation of the MAPK-linked NF-κB signaling pathway axis in mice liver.[51] Similarly, lipid accumulation in the MG accompanies HFD-induced pathophysiological responses. Recent studies have shown that a HFD was associated with macrophage recruitment in adipose tissue.[26,27] Rises in F4/80 staining in the MG of mice on a HFD stemmed from increases in macrophage infiltration mediated by HFD-induced NF-κB activation.[52] Increases in CD45-stained immune cells delimited in the periglandular region correlated with the severity of the inflammatory condition within the MG of mice fed a HFD.

The increases in lipid accumulation occurring during prolonged periods on the HFD were identified based on progressive increases in LipidTox staining in acinar units. Activation of inflammatory cytokines such as TNF-α, IL-1, IL-6, and NF-κB could promote cell apoptosis.[53–55] The inflammatory condition accompanying such rises in lipids may contribute to inducing MG cellular apoptosis. On the other hand, the increases in MG cell death could instead underlie dysregulation of MG physiological processes such as lipogenesis, lipid clearance, and lipolysis, leading to lipid accumulation in the mice fed the HFD. Further insight into hyperlipidemia-related MGD awaits the analysis of meibum and tear lipid composition in the mice fed a HFD. HFD-induced activation increased ERK1/2, p38, and JNK/MAPK phosphorylation, whereas PPAR-γ expression levels were downregulated. These effects contribute to the cell structural changes and the inflammatory condition induced by the HFD. Other studies involving immune cells have shown that p38 MAPK regulates TNF-α, IL-1β, IL-6, and IL-8 cytokine expression levels, which in turn trigger immune responses.[56] Previous studies have shown that MAPKs play critical roles

Investigative Ophthalmology & Visual Science

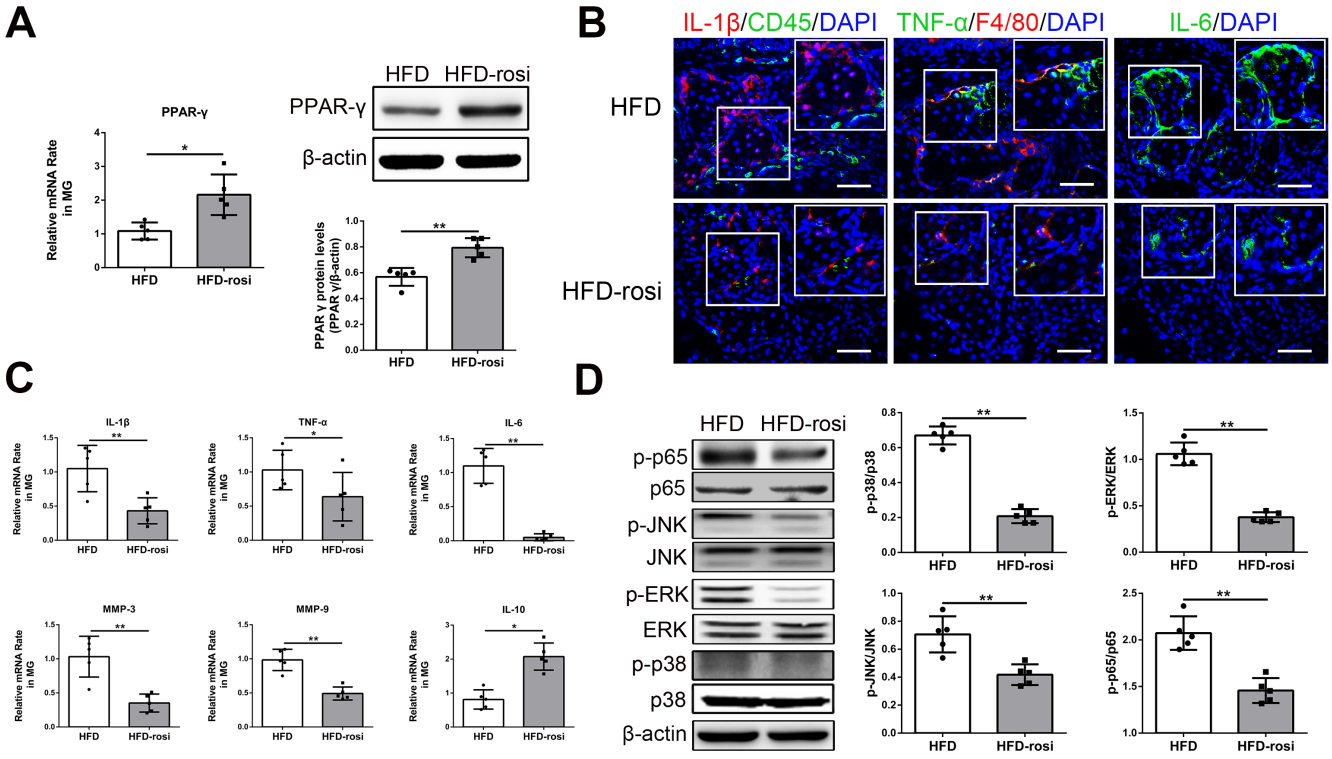

Figure 7. Rosiglitazone decreased HFD-induced MG inflammation. (**A**) Quantitative RT-PCR and western blot analyses show increased PPAR-γ gene and protein expression levels in mice placed on the HFD and were treated simultaneously with rosiglitazone. (**B**) Immunofluorescent staining shows decreased IL-1β, CD45, TNF-α, F4/80, and IL-6 expression levels in the rosiglitazone-treated group. (**C**) Quantitative RT-PCR analysis shows that rosiglitazone downregulated IL-1β, IL-6, and TNF-α expression levels, whereas IL-10 expression was upregulated. (**D**) Western blot analysis shows that rosiglitazone induced declines in MAPK and NF-κB p65 phosphorylation. *Scale bars*: 50 µm. Data are shown as mean ± SD; $n = 5$; $^{*}P < 0.05$, $^{**}P < 0.01$. ROSI, rosiglitazone.

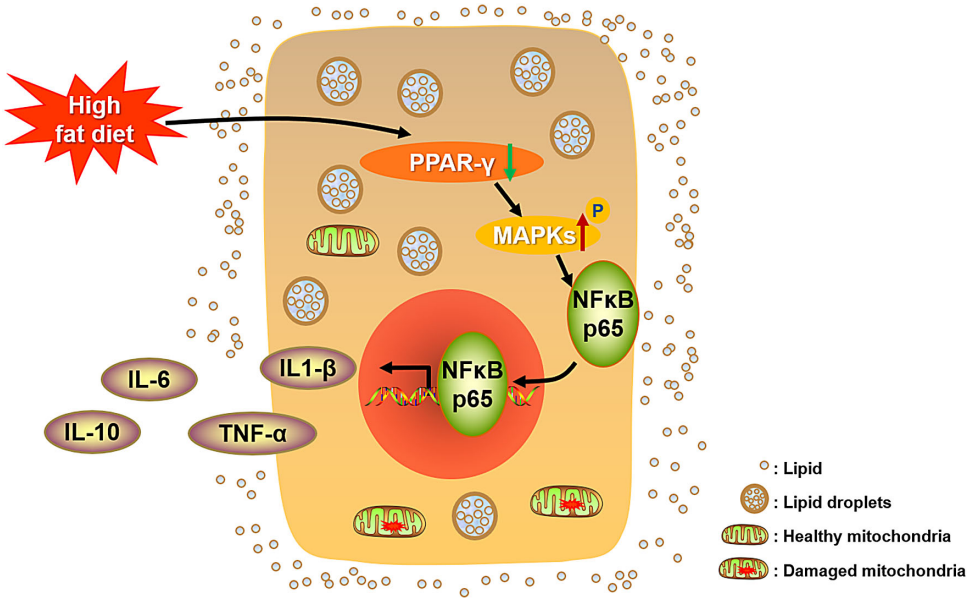

Figure 8. Illustration of the hypothetical mechanism of MG inflammation following a HFD.

in the regulation of HFD-induced inflammation.[57–59] In our study, when we switch the mice from the HFD to the SD, the activation of MAPKs was suppressed. Phosphorylation of *c*-Jun amino-terminal kinase and p38 have been shown to be diminished in heterozygous PPAR-γ–deficient (*PPAR-*$\gamma^{+/-}$) mice in response to specific stimuli.[60] Furthermore, in inflammatory bowel disease, activating PPAR-γ suppressed proinflammatory cytokine and chemokine expression levels

Investigative Ophthalmology & Visual Science

by reducing MAPK and NF-κB activation.[61] PPAR-γ agonist could inhibit advanced glycation end product–induced chondrocytes apoptosis and degeneration by suppressing the activation of MAPK and NF-κB.[62] In our study, rosiglitazone increased the PPAR-γ expression level, suppressed MAPK and NF-κB cascade activation, and inhibited rises in the proinflammatory cytokine expression levels, indicating that MAPKs were likely downstream of PPAR-γ in HFD-induced MG inflammation.

The role of PPAR-γ in controlling cell signaling events mediating HFD-induced increases in MG inflammatory status is consistent with its involvement in other physiological processes. This transcription factor is an important regulator of sebocyte maturation in the sebaceous gland,[63] as well as meibocyte differentiation and lipid synthesis.[64] PPAR-γ also plays a key role in anti-inflammation.[65] In our study, rosiglitazone, a specific agonist of PPAR-γ, reversed the PPAR-γ declines toward normal levels, which offset HFD-induced increases in macrophage infiltration and rises in proinflammatory cytokine and chemokine expression levels in the MG, indicating that HFD-induced PPAR-γ downregulation may account for the elevated inflammatory cell infiltration and upregulation of proinflammatory cytokine gene and protein expression. Moreover, the pathophysiological impact of the HFD on the MG was substantiated based on observing that these deleterious effects were reversed by switching from the HFD to the SD.

We found lipid accumulation in the MG, and the expression of PPAR-γ decreased after the HFD. Consistent with another study by our group, PPAR-γ expression was also decreased and lipid accumulation increased in an ApoE knockout MGD animal model.[9] Illesca et al.[66] reported that a HFD can lead to downregulation of PPAR-γ expression accompanied with upregulation of transcription factors and their target genes involved in lipogenesis in adipose tissue. A HFD can also lead to downregulation of PPAR-γ expression in the small intestine.[67] In our current study, PPAR-γ expression decreased with the HFD, accompanied by lipid accumulation in the MG, perhaps due in part to the activation of other genes involved in lipogenesis in MG. Additionally, obstruction of the MG, the most prominent aspect of MGD,[19] would lead to lipid accumulation in the MG duct and acinar. Moreover, increased LipidTox staining may represent the accumulation of other abnormal lipids. We will investigate this further in our future study. In this study, rosiglitazone partially offset HFD-induced increases of proinflammatory cytokine and chemokine expression levels in the MG, indicating that HFD-induced PPAR-γ downregulation may be responsible for the elevated inflammatory cell infiltration and upregulation of proinflammatory cytokine expression. Therefore, PPAR-γ was involved not only in lipid synthesis but also anti-inflammation in our study.

Our previous study showed that a HFD could induce corneal epithelial barrier disruption and significant squamous metaplasia of the corneal epithelia, leading to dry eye–like ocular surface damage.[8] Another study from our group showed that a HFD induced abnormal lipid accumulation, inflammation, lipid peroxidation, and apoptosis in the lacrimal gland, leading to declines in aqueous tear secretion.[44] The aqueous tear secretion was reduced to about half of the normal level after 4 months on a HFD, based on our previous study. In our current study, inflammation of the MG was also evident, and there was a milky secretion on the eyelid margin after 4 months on the HFD. Therefore, we suspect that both aqueous tear deficiency and MG dysfunction contribute to the dry eye–like ocular surface changes in mice fed a HFD.

It remains unclear whether MG inflammation is a primary or secondary response to systemic inflammation induced by a HFD. It is also unknown whether a HFD induces ocular surface inflammation, which would then compromise MG dysfunction. Because MGs are easily accessible for determining phenotypic changes, they are an attractive tissue for use in clarifying the relationship between a HFD and inflammation.

In conclusion, HFD-induced hyperlipidemia promoted MG inflammation through concurrent PPAR-γ downregulation and upregulation of the MAPK/NF-κB signaling pathway axis, followed by increases in inflammatory cell infiltration and rises in MG proinflammatory cytokine gene and protein expression in mice (Fig. 8). Our study provided direct and extended evidence of HFD-induced MG inflammation, largely in response to an alteration of PPAR-γ signaling, thus suggesting that PPAR-γ may be a potential treatment target with regard to MG inflammation induced by a HFD. Diet control may be a possible therapeutic strategy for HFD-related MGD inhibition and treatment.

Acknowledgments

The authors thank Kechun Li from the University of Minnesota for the animal feeding and care.

Supported in part by grants from the National Key R&D Program of China (2018YFA0107301 to WL, 2018YFA0107304 to ZL) and the National Natural Science Foundation of China (81970773 and 81770894 to WL, 82000868 to JB, 82000856 to YW). The funders had no role in the study design, data collection and analysis, decision on publishing, or preparation of the manuscript.

Disclosure: **J. Bu**, None; **M. Zhang**, None; **Y. Wu**, None; **N. Jiang**, None; **Y. Guo**, None; **X. He**, None; **H. He**, None; **M.V. Jeyalatha**, None; **P.S. Reinach**, None; **Z. Liu**, None; **W. Li**, None

References

1. Goff DC, Jr, Bertoni AG, Kramer H, et al. Dyslipidemia prevalence, treatment, and control in the Multi-Ethnic Study of Atherosclerosis (MESA): gender, ethnicity, and coronary artery calcium. *Circulation*. 2006;113:647–656.
2. Centers for Disease Control and Prevention. Vital signs: prevalence, treatment, and control of high levels of low-density lipoprotein cholesterol–United States, 1999-2002 and 2005-200. *MMWR Morb Mortal Wkly Rep*. 2011;60:109–114.
3. Mozaffarian D, Benjamin EJ, Go AS, et al. Heart disease and stroke statistics-2016 update: a report from the American Heart Association. *Circulation*. 2016;133:e38–e360.
4. Smith DG. Epidemiology of dyslipidemia and economic burden on the healthcare system. *Am J Manag Care*. 2007;13(suppl 3):S68–S71.
5. El-Tantawy WH, Temraz A. Natural products for controlling hyperlipidemia: review. *Arch Physiol Biochem*. 2019;125:128–135.
6. Alberti KG, Eckel RH, Grundy SM, et al. Harmonizing the metabolic syndrome: a joint interim statement of the International Diabetes Federation Task Force on Epidemiology and Prevention; National Heart, Lung, and Blood Institute; American Heart Association; World Heart Federation; International Atherosclerosis Society; and International

Association for the Study of Obesity. *Circulation*. 2009;120:1640–1645.
7. Mozaffarian D, Benjamin EJ, Go AS, et al. Heart disease and stroke statistics–2015 update: a report from the American Heart Association. *Circulation*. 2015;131:e29–322.
8. Wu Y, Wu J, Bu J, et al. High-fat diet induces dry eye-like ocular surface damages in murine. *Ocul Surf*. 2020;18:267–276.
9. Bu J, Wu Y, Cai X, et al. Hyperlipidemia induces meibomian gland dysfunction. *Ocul Surf*. 2019;17:777–786.
10. Expert Panel on Detection, Evaluation, and Treatment of High Blood Cholesterol in Adults. Executive Summary of the Third Report of the National Cholesterol Education Program (NCEP) Expert Panel on Detection, Evaluation, and Treatment of High Blood Cholesterol in Adults (Adult Treatment Panel III). *JAMA*. 2001;285:2486–2497.
11. Che X, Wu H, Jia C, et al. A novel tissue-engineered corneal stromal equivalent based on amniotic membrane and keratocytes. *Invest Ophthalmol Vis Sci*. 2019;60:517–527.
12. Jester JV, Potma E, Brown DJ. PPARγ regulates mouse meibocyte differentiation and lipid synthesis. *Ocul Surf*. 2016;14:484–494.
13. Tokutome M, Matoba T, Nakano Y, et al. Peroxisome proliferator-activated receptor-gamma targeting nanomedicine promotes cardiac healing after acute myocardial infarction by skewing monocyte/macrophage polarization in preclinical animal models. *Cardiovasc Res*. 2019;115:419–431.
14. Kiss M, Czimmerer Z, Nagy L. The role of lipid-activated nuclear receptors in shaping macrophage and dendritic cell function: from physiology to pathology. *J Allergy Clin Immunol*. 2013;132:264–286.
15. Arita R, Fukuoka S, Morishige N. New insights into the morphology and function of meibomian glands. *Exp Eye Res*. 2017;163:64–71.
16. Tomas J, Mulet C, Saffarian A, et al. High-fat diet modifies the PPAR-γ pathway leading to disruption of microbial and physiological ecosystem in murine small intestine. *Proc Natl Acad Sci USA*. 2016;113:E5934–E5943.
17. Benzler J, Ganjam GK, Pretz D, et al. Central inhibition of IKKβ/NF-κB signaling attenuates high-fat diet-induced obesity and glucose intolerance. *Diabetes*. 2015;64:2015–2027.
18. Jeyalatha MV, Qu Y, Liu Z, et al. Function of meibomian gland: contribution of proteins. *Exp Eye Res*. 2017;163:29–36.
19. Nelson JD, Shimazaki J, Benitez-del-Castillo JM, et al. The international workshop on meibomian gland dysfunction: report of the definition and classification subcommittee. *Invest Ophthalmol Vis Sci*. 2011;52:1930–1937.
20. Bron AJ, Tiffany JM. The contribution of meibomian disease to dry eye. *Ocul Surf*. 2004;2:149–165.
21. Nien CJ, Paugh JR, Massei S, Wahlert AJ, Kao WW, Jester JV. Age-related changes in the meibomian gland. *Exp Eye Res*. 2009;89:1021–1027.
22. Wolffsohn JS, Arita R, Chalmers R, et al. TFOS DEWS II Diagnostic Methodology report. *Ocul Surf*. 2017;15:539–574.
23. Hotamisligil GS, Shargill NS, Spiegelman BM. Adipose expression of tumor necrosis factor-alpha: direct role in obesity-linked insulin resistance. *Science*. 1993;259:87–91.
24. Hotamisligil GS. Inflammation and metabolic disorders. *Nature*. 2006;444:860–867.
25. Buckman LB, Hasty AH, Flaherty DK, et al. Obesity induced by a high-fat diet is associated with increased immune cell entry into the central nervous system. *Brain Behav Immun*. 2014;35:33–42.
26. Weisberg SP, McCann D, Desai M, Rosenbaum M, Leibel RL, Ferrante AW, Jr. Obesity is associated with macrophage accumulation in adipose tissue. *J Clin Invest*. 2003;112:1796–1808.
27. Xu H, Barnes GT, Yang Q, et al. Chronic inflammation in fat plays a crucial role in the development of obesity-related insulin resistance. *J Clin Invest*. 2003;112:1821–1830.
28. Li S, Zeng XY, Zhou X, et al. Dietary cholesterol induces hepatic inflammation and blunts mitochondrial function in the liver of high-fat-fed mice. *J Nutr Biochem*. 2016;27:96–103.
29. Yuan Y, Naito H, Jia X, Kitamori K, Nakajima T. Combination of hypertension along with a high fat and cholesterol diet induces severe hepatic inflammation in rats via a signaling network comprising NF-κB, MAPK, and Nrf2 pathways. *Nutrients*. 2017;9:1018.
30. Ishimoto T, Lanaspa MA, Rivard CJ, et al. High-fat and high-sucrose (western) diet induces steatohepatitis that is dependent on fructokinase. *Hepatology*. 2013;58:1632–1643.
31. van der Heijden RA, Sheedfar F, Morrison MC, et al. High-fat diet induced obesity primes inflammation in adipose tissue prior to liver in C57BL/6j mice. *Aging (Albany NY)*. 2015;7:256–268.
32. Pirchl M, Ullrich C, Sperner-Unterweger B, Humpel C. Homocysteine has anti-inflammatory properties in a hypercholesterolemic rat model in vivo. *Mol Cell Neurosci*. 2012;49:456–463.
33. Hansson GK. Inflammation, atherosclerosis, and coronary artery disease. *N Engl J Med*. 2005;352:1685–1695.
34. Cox AJ, West NP, Cripps AW. Obesity, inflammation, and the gut microbiota. *Lancet Diabetes Endocrinol*. 2015;3:207–215.
35. Wang S, Bao X. Hyperlipidemia, blood lipid level, and the risk of glaucoma: a meta-analysis. *Invest Ophthalmol Vis Sci*. 2019;60:1028–1043.
36. Shen J, He J, Wang F. Association of lipids with age-related macular degeneration. *Discov Med*. 2016;22:129–145.
37. Kowluru RA, Mishra M, Kowluru A, Kumar B. Hyperlipidemia and the development of diabetic retinopathy: comparison between type 1 and type 2 animal models. *Metabolism*. 2016;65:1570–1581.
38. Tsutsumi K, Inoue Y, Yoshida C. Acceleration of development of diabetic cataract by hyperlipidemia and low high-density lipoprotein in rats. *Biol Pharm Bull*. 1999;22:37–41.
39. Collins KH, Herzog W, Reimer RA, Reno CR, Heard BJ, Hart DA. Diet-induced obesity leads to pro-inflammatory alterations to the vitreous humour of the eye in a rat model. *Inflamm Res*. 2018;67:139–146.
40. Lee JJ, Wang PW, Yang IH, et al. High-fat diet induces toll-like receptor 4-dependent macrophage/microglial cell activation and retinal impairment. *Invest Ophthalmol Vis Sci*. 2015;56:3041–3050.
41. Huang X, Li Y, Fu M, Xin HB. Polarizing macrophages in vitro. *Methods Mol Biol*. 2018;1784:119–126.
42. Siouti E, Andreakos E. The many facets of macrophages in rheumatoid arthritis. *Biochem Pharmacol*. 2019;165:152–169.
43. Stienstra R, Duval C, Keshtkar S, van der Laak J, Kersten S, Müller M. Peroxisome proliferator-activated receptor gamma activation promotes infiltration of alternatively activated macrophages into adipose tissue. *J Biol Chem*. 2008;283:22620–22627.
44. He X, Zhao Z, Wang S, et al. High-fat diet-induced functional and pathologic changes in lacrimal gland. *Am J Pathol*. 2020;190:2387–2402.
45. Celinski K, Dworzanski T, Korolczuk A, et al. Effects of peroxisome proliferator-activated receptors-gamma ligands on dextran sodium sulphate-induced colitis in rats. *J Physiol Pharmacol*. 2011;62:347–356.

Investigative Ophthalmology & Visual Science

46. Pisanu A, Lecca D, Mulas G, et al. Dynamic changes in pro- and anti-inflammatory cytokines in microglia after PPAR-γ agonist neuroprotective treatment in the MPTPp mouse model of progressive Parkinson's disease. *Neurobiol Dis*. 2014;71:280–291.
47. Acera A, Vecino E, Duran JA. Tear MMP-9 levels as a marker of ocular surface inflammation in conjunctivochalasis. *Invest Ophthalmol Vis Sci*. 2013;54:8285–8291.
48. Chintala SK, Zhang X, Austin JS, Fini ME. Deficiency in matrix metalloproteinase gelatinase B (MMP-9) protects against retinal ganglion cell death after optic nerve ligation. *J Biol Chem*. 2002;277:47461–47468.
49. Ding J, Kam WR, Dieckow J, Sullivan DA. The influence of 13-cis retinoic acid on human meibomian gland epithelial cells. *Invest Ophthalmol Vis Sci*. 2013;54:4341–4350.
50. Ogata Y, Enghild JJ, Nagase H. Matrix metalloproteinase 3 (stromelysin) activates the precursor for the human matrix metalloproteinase 9. *J Biol Chem*. 1992;267:3581–3584.
51. Cai D, Yuan M, Frantz DF, et al. Local and systemic insulin resistance resulting from hepatic activation of IKK-beta and NF-kappaB. *Nat Med*. 2005;11:183–190.
52. Trowbridge IS, Thomas ML. CD45: an emerging role as a protein tyrosine phosphatase required for lymphocyte activation and development. *Annu Rev Immunol*. 1994;12:85–116.
53. Santamaría B, Ucero AC, Benito-Martin A, et al. Biocompatibility reduces inflammation-induced apoptosis in mesothelial cells exposed to peritoneal dialysis fluid. *Blood Purif*. 2015;39:200–209.
54. Meng Q-T, Chen R, Chen C, et al. Transcription factors Nrf2 and NF-κB contribute to inflammation and apoptosis induced by intestinal ischemia-reperfusion in mice. *Int J Mol Med*. 2017;40:1731–1740.
55. Satoh A, Gukovskaya AS, Edderkaoui M, et al. Tumor necrosis factor-α mediates pancreatitis responses in acinar cells via protein kinase C and proline-rich tyrosine kinase 2. *Gastroenterology*. 2005;129:639–651.
56. Johnson GL, Lapadat R. Mitogen-activated protein kinase pathways mediated by ERK, JNK, and p38 protein kinases. *Science*. 2002;298:1911–1912.
57. Chen X, Yu W, Li W, et al. An anti-inflammatory chalcone derivative prevents heart and kidney from hyperlipidemia-induced injuries by attenuating inflammation. *Toxicol Appl Pharmacol*. 2018;338:43–53.
58. Mi Y, Qi G, Fan R, et al. EGCG ameliorates high-fat- and high-fructose-induced cognitive defects by regulating the IRS/AKT and ERK/CREB/BDNF signaling pathways in the CNS. *Faseb J*. 2017;31:4998–5011.
59. Bargut TC, Mandarim-de-Lacerda CA, Aguila MB. A high-fish-oil diet prevents adiposity and modulates white adipose tissue inflammation pathways in mice. *J Nutr Biochem*. 2015;26:960–969.
60. Desreumaux P, Dubuquoy L, Nutten S, et al. Attenuation of colon inflammation through activators of the retinoid X receptor (RXR)/peroxisome proliferator-activated receptor gamma (PPARgamma) heterodimer. A basis for new therapeutic strategies. *J Exp Med*. 2001;193:827–838.
61. Choo J, Lee Y, Yan XJ, et al. A novel peroxisome proliferator-activated receptor (PPAR)γ agonist 2-hydroxyethyl 5-chloro-4,5-didehydrojasmonate exerts anti-inflammatory effects in colitis. *J Biol Chem*. 2015;290:25609–25619.
62. Zhang HB, Zhang Y, Chen C, Li YQ, Ma C, Wang ZJ. Pioglitazone inhibits advanced glycation end product-induced matrix metalloproteinases and apoptosis by suppressing the activation of MAPK and NF-κB. *Apoptosis*. 2016;21:1082–1093.
63. Dozsa A, Dezso B, Toth BI, et al. PPARγ-mediated and arachidonic acid-dependent signaling is involved in differentiation and lipid production of human sebocytes. *J Invest Dermatol*. 2014;134:910–920.
64. Hwang HS, Parfitt GJ, Brown DJ, Jester JV. Meibocyte differentiation and renewal: insights into novel mechanisms of meibomian gland dysfunction (MGD). *Exp Eye Res*. 2017;163:37–45.
65. Zingarelli B, Cook JA. Peroxisome proliferator-activated receptor-gamma is a new therapeutic target in sepsis and inflammation. *Shock*. 2005;23:393–399.
66. Illesca P, Valenzuela R, Espinosa A, et al. Hydroxytyrosol supplementation ameliorates the metabolic disturbances in white adipose tissue from mice fed a high-fat diet through recovery of transcription factors Nrf2, SREBP-1c, PPAR-γ and NF-κB. *Biomed Pharmacother*. 2019;109:2472–2481.
67. Sferra R, Pompili S, Cappariello A, Gaudio E, Latella G, Vetuschi A. Prolonged chronic consumption of a high fat with sucrose diet alters the morphology of the small intestine. *Int J Mol Sci*. 2021;22.

Investigative Ophthalmology & Visual Science